ADVANCED FUNCTIONAL MATERIALS
www.afm-journal.de

One-Step Macroscopic Alignment of Conjugated Polymer Systems by Epitaxial Crystallization during Spin-Coating

Christian Müller, Mahdieh Aghamohammadi, Scott Himmelberger, Prashant Sonar, Miquel Garriga, Alberto Salleo, and Mariano Campoy-Quiles*

The one-step preparation of highly anisotropic polymer semiconductor thin films directly from solution is demonstrated. The conjugated polymer poly(3-hexylthiophene) (P3HT) as well as P3HT:fullerene bulk–heterojunction blends can be spin-coated from a mixture of the crystallizable solvent 1,3,5-trichlorobenzene (TCB) and a second carrier solvent such as chlorobenzene. Solidification is initiated by growth of macroscopic TCB spherulites followed by epitaxial crystallization of P3HT on TCB crystals. Subsequent sublimation of TCB leaves behind a replica of the original TCB spherulites. Thus, highly ordered thin films are obtained, which feature square-centimeter-sized domains that are composed of one spherulite-like structure each. A combination of optical microscopy and polarized photoluminescence spectroscopy reveals radial alignment of the polymer backbone in case of P3HT, whereas P3HT:fullerene blends display a tangential orientation with respect to the center of spherulite-like structures. Moreover, grazing-incidence wide-angle X-ray scattering reveals an increased relative degree of crystallinity and predominantly flat-on conformation of P3HT crystallites in the blend. The use of other processing methods such as dip-coating is also feasible and offers uniaxial orientation of the macromolecule. Finally, the applicability of this method to a variety of other semi-crystalline conjugated polymer systems is established. Those include other poly(3-alkylthiophene)s, two polyfluorenes, the low band-gap polymer PCPDTBT, a diketopyrrolopyrrole (DPP) small molecule as well as a number of polymer:fullerene and polymer:polymer blends.

1. Introduction

Conjugated polymers currently attract considerable interest for use in thin-film solar cells, light-emitting diodes (LEDs) and electronic circuitry.[1–3] Large-area processing techniques such as printing and coating are desired since they promise to be particularly cost-efficient. However, film formation from solution typically results in an inconveniently high degree of disorder accompanied by a micro- or even nanoscopic domain size. Unfortunately, the large number of grain boundaries tends to impede electronic charge transport and the limited domain size randomizes the high optical anisotropy that is intrinsic to conjugated polymer chains. Thus, a variety of thin-film alignment techniques have been developed that permit uniaxial orientation or at least preparation of macroscopic domains. Those include the introduction of liquid-crystal alignment layers,[4,5] the use of rubbed polytetrafluoroethylene (PTFE) transfer layers[6,7] or organic "substrates" such as crystallizable solvents for epitaxy,[8–12] mechanical rubbing,[13] stretching of a plastic substrate,[14–16] imprinting,[17,18] Langmuir–Blodgett deposition[19] and even vapor annealing.[20,21] Without doubt, utilization of such methods not only eases the study of fundamental optoelectronic processes but has triggered interest in technological applications such as polarized LEDs.[4,7,13,19]

An emerging concept is to use alignment techniques to structure organic semiconductor blends. Those are of high relevance for a variety of applications such as polymer solar cells that are based on polymer:fullerene bulk–heterojunction blends. Currently, the majority of studies focus on increasing the power conversion efficiency of such devices. For this purpose, in-plane alignment of the active materials is not considered to be of relevance. However, Vohra et al. have recently demonstrated that the device performance of graded bilayer P3HT:[6,6]-phenyl-C_{61}-butyric acid methyl ester ($PC_{61}BM$) solar cells can be substantially improved by in-plane alignment of the polymer through mechanical rubbing.[22] The authors rationalized this observation with improved charge-transport in the vertical direction, which was facilitated by improved face-on orientation of P3HT.

Dr. C. Müller,[+] M. Aghamohammadi, Dr. M. Garriga, Dr. M. Campoy-Quiles
Institut de Ciència de Materials de Barcelona (ICMAB-CSIC)
Esfera de la UAB, 08193 Bellaterra, Spain
E-mail: christian.muller@chalmers.se
S. Himmelberger, Prof. A. Salleo
Department of Materials Science and Engineering
Stanford University
Stanford, CA 94305, USA
Dr. P. Sonar
Institute of Materials Research and Engineering (IMRE)
Agency for Science, Technology and Research (A*STAR)
3, Research Link, 117602, Singapore
[+] Present address: Department of Chemical and Biological Engineering/Polymer Technology, Chalmers University of Technology, 41296 Göteborg, Sweden

DOI: 10.1002/adfm.201202983

This dependency is in agreement with a recent report by Gomez et al. who showed that a high degree of out-of-plane π-stacking is desired for P3HT:$PC_{61}BM$ solar cells since the obtainable short-circuit current strongly correlates with this crystal conformation.[23] Moreover, the design of polymer solar cells that feature pronounced optical anisotropy can facilitate device concepts that go beyond simple light-harvesting applications. Recently, such a device was reported by Zhu et al. who prepared polarizing polymer solar cells by mechanical rubbing of a P3HT thin film followed by spin-coating a top layer of $PC_{61}BM$ from dichloromethane.[24] The authors proposed that such a device could be used as a polarizing filter in liquid-crystal displays that harvests at least some of the backlight, which is usually lost. Besides practical applications, oriented bulk–heterojunctions can assist in fundamental photo-physical studies. For instance, Vandewal et al. recently fabricated polarized solar cells, again by mechanical rubbing of polymer thin films, to probe the polarization anisotropy of charge-transfer absorption and emission.[25] Currently, mechanical rubbing is the only technique that has been used to align bulk–heterojunction blends. Clearly, the development of additional methods that can be more readily adapted to solution processing would offer significant advantages, not only for the design of polarized solar cells but also bipolar field-effect transistors and white LEDs.

Among the above discussed alignment techniques, the use of a crystallizable solvent is particularly versatile. Key is the selection of a suitable compound, which initially dissolves the polymer and then crystallizes to induce epitaxial solidification of the macromolecule. This approach was originally developed by Wittmann and Lotz who used aromatic compounds such as benzoic acid in combination with polyethylene.[26] Brinkmann et al. adopted this method to directionally solidify conjugated polymers such as poly(3-hexylthiophene) (P3HT) and poly(9,9-dioctylfluorene) (PFO) with 1,3,5-trichlorobenzene (TCB) as the crystallizable solvent, which elegantly confirmed their semicrystalline nature.[8–11] Moreover, Jimison et al. were able to fabricate field-effect transistors with directionally crystallized P3HT and used those devices to explore the interplay of orientation, grain boundaries and electronic charge transport.[12] In principle, this method is compatible with a wide range of substrates and device configurations since no alignment layers are required. However, a laborious sequence of processing steps has to be followed after initial film formation, which limits the practicality of this technique. First, the crystallized solvent is placed on the semiconductor film followed by a top substrate to confine the two materials. Subsequent heating melts the aromatic compound, which in turn dissolves the conjugated polymer to form a continuous wetting layer. Then, application of a temperature gradient can be used to directionally solidify the polymer–solvent system. Finally, the re-crystallized solvent is permitted to evaporate in order to retain a semiconductor-only thin film. Evidently, the recipe in its current form cannot permit rapid solution processing over a large area.

Here, we demonstrate that the crystallizable solvent technique can be adapted to align not only single-component systems but also polymer–fullerene bulk–heterojunction blends. Instead of following previously published processing routines, we have developed a modified approach that facilitates the one-step preparation of highly anisotropic thin films directly from solution. We achieve this through *co*-deposition of the semiconductor blend and crystallizable solvent from a second carrier solvent. This approach permits fabrication of continuous thin films by spin- or dip-coating that display pronounced in-plane alignment. Intriguingly, we observe macroscopic spherulite-like structures that resemble those readily formed by non-conjugated polymers but are usually absent in conjugated polymer thin films unless the nucleation density is carefully controlled.[20,21] Moreover, we show that our technique is applicable to a wide range of semicrystalline organic semiconductor systems, including different conjugated polymers and a small molecule as well as a number of polymer–fullerene and polymer–polymer blends.

2. Results and Discussion

Initially, we focused our study on P3HT, which is one of the most-widely studied polymer semiconductors. We used regioregular P3HT with a weight-average molecular weight $M_w \approx 48$ kg mol^{-1} that is considered to be sufficiently high for chain folding to occur.[9] Alongside, we investigated bulk–heterojunction blends of P3HT and $PC_{61}BM$ because of the wide interest in this particular system for organic solar cells.

In a first set of experiments, we examined thin films of P3HT and P3HT:$PC_{61}BM$ spin-coated from solvent mixtures of chlorobenzene (CB) and TCB (cf. **Figure 1**a for chemical structures). We added an increasing amount of crystallizable solvent to a fixed ratio of solute and CB. Thus, we systematically explored fractions from 0–16 vol% TCB.[27] Reference samples prepared from CB display no birefringence as evidenced by the cross-polarized micrographs shown in Figure 1b. In most significant contrast, thin films spin-coated from solvent mixtures that contained more than ≈4 vol% TCB feature pronounced Maltese-cross patterns that are characteristic of polymer spherulites (cf. Supporting Information Figure S1a for additional micrographs; note that this threshold appeared to be independent of the P3HT concentration). We rationalize this change in solidification behavior with a variation in the crystallization sequence of TCB and P3HT during evaporation of the more volatile CB carrier solvent. For a low TCB concentration of less than 4 vol%, the polymer continues to solidify from solution and TCB merely acts as a high boiling point solvent additive similar to the nitrobenzene/CB solvent mixture investigated by Moulé and Meerholz[28] or the 1,8-octanedithiol/1,2-dichlorobenezene system explored by Yao et al.[29] In this regime we observe an enhancement in P3HT crystallinity as evidenced by the pronounced red-shift in UV-vis absorbance as well as rise in the absorbance shoulder at 610 nm relative to the absorbance peak at 555 nm, which according to Spano et al. correlates with increased π-stacking of the polymer (Supporting Information Figure S1b).[30] The increase in polymer ordering is most pronounced in P3HT:$PC_{61}BM$ blends. This suggests that the use of TCB as a solvent additive has a comparable effect as thermal annealing, which is usually required to achieve optimum photovoltaic performance with this blend in bulk–heterojunction solar cells. Here, we would like to draw attention to the work by Keawprajak et al., who studied P3HT:$PC_{61}BM$ devices prepared with up to 4 vol% TCB and obtained a moderate improvement in power conversion efficiency.[31]

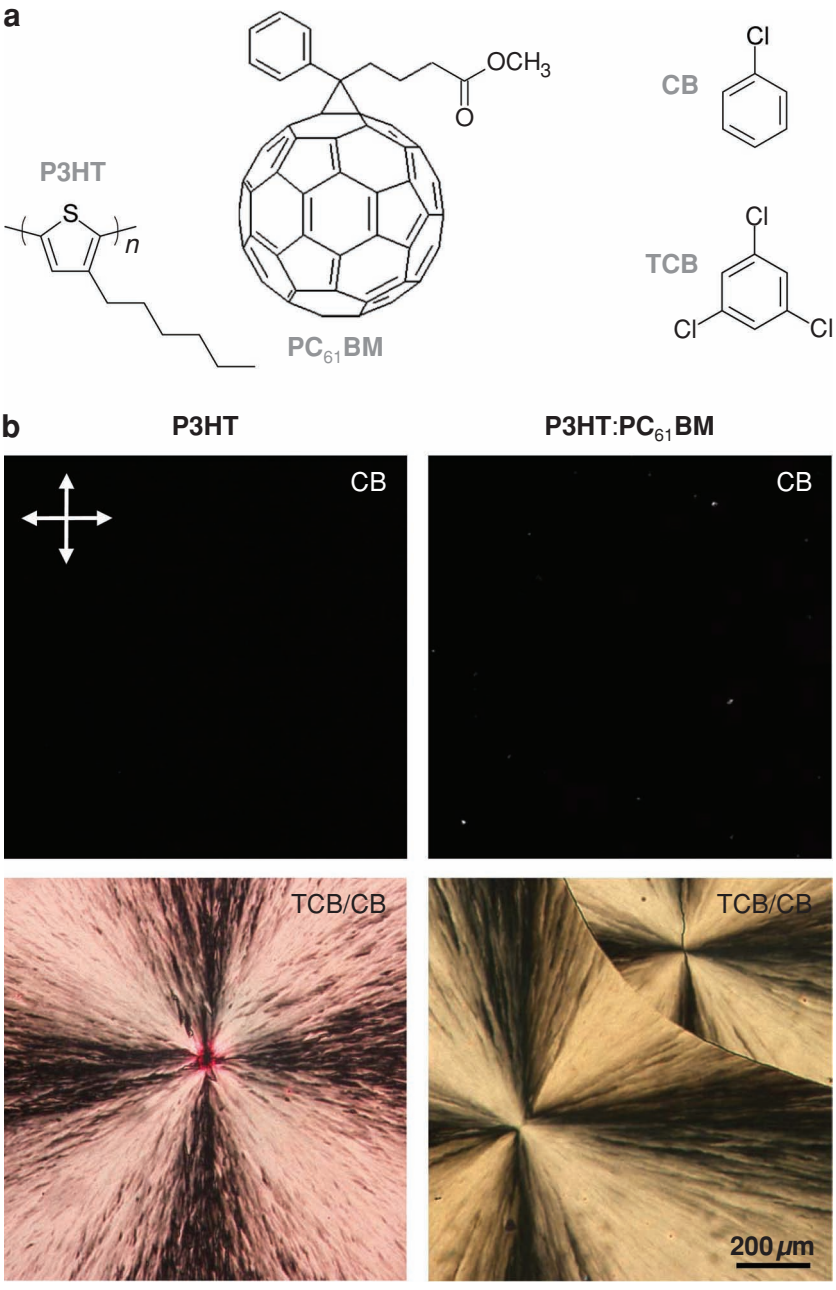

Figure 1. Chemical structures and appearance of spin-coated thin films. a) Chemical structure of P3HT and $PC_{61}BM$ (left) as well as the solvents CB and TCB (right). b) Cross-polarized optical micrographs of P3HT (left) and 1:1 P3HT:$PC_{61}BM$ thin films (right) that were spin-coated from CB (top) and TCB/CB (7.5 and 10 vol% TCB, respectively; bottom). Orientation of the polarizer pair indicated by white arrows.

Solutions with a higher TCB concentration above 4 vol% show a markedly different solidification behavior. In this regime, the crystallizable solvent already starts to solidify while P3HT is still in solution and grows crystals that initiate from a common nucleus to form TCB spherulites. Subsequent to TCB crystallization, epitaxial solidification of the polymer on TCB crystals leads to the spherulite-like arrangement of P3HT. These P3HT structures are retained after sublimation of TCB and thus replicate the original crystallized solvent spherulites.

Here, we would like to point out that the low nucleation density of TCB, which is approximately equal to the number of spherulite centers, is not equal to the nucleation density of P3HT. P3HT solidification is driven by epitaxy with the surface of TCB crystals. Generally, for this mode of crystallization the nucleation density of polymers increases as lattice matching is approached. Thus, we conclude that the nucleation density of P3HT is likely to be even higher than in reference P3HT processed from CB (cf. Ref. [26] and discussion below on the good lattice matching of TCB and P3HT crystals).

The number of spherulite-like structures could be controlled by adjusting the volume fraction of TCB with respect to both, the carrier solvent and the polymer content. We chose to keep a fixed P3HT content of 20 g L^{-1} and systematically varied the TCB concentration. Under these conditions the number of spherulite-like structures in the final films is extremely low, which we assume to be equal to the nucleation density of TCB spherulites. We find a maximum nucleation density at 7.5 vol% TCB for P3HT and at 10 vol% TCB for P3HT:$PC_{61}BM$ with approximately 4–5 nuclei per square-centimeter and a slightly lower nucleation density of about 2 nuclei cm^{-2} at higher TCB concentrations (Supporting Information Figure S2). As a result, we obtain macroscopic domains that are composed of one spherulite-like structure each. For a given concentration of TCB/CB and polymer the nucleation density did not appear to differ when spin-coating on different substrates such as glass, PEDOT:PSS coated glass or silicon wafers. This observation implies that TCB crystal nucleation is largely independent of the choice of substrate and thus predominantly occurs throughout the thin film.

Although sublimation of TCB appeared to readily proceed at ambient conditions, we exposed the samples to a mild vacuum in order to remove any trace solvent. Attenuated total reflectance infra-red (ATR-IR) spectroscopy confirmed that the solidified films were solely composed of the semiconductor as judged by the absence of prominent IR signals of TCB at 3083, 1095, 847, 812, and 795 cm^{-1} (Supporting Information Figure S3). In addition, the absence of significant shifts in the IR peak positions and the absence of new peaks indicates that no stable P3HT:TCB compounds are formed. The spin-coated films had a thickness of about 160 nm, which appeared insensitive to the amount of TCB in the initial solution. Moreover, we employed atomic force microscopy (AFM) to confirm that samples spin-coated from, e.g., 7.5–10 vol% TCB provide a continuous surface coverage.

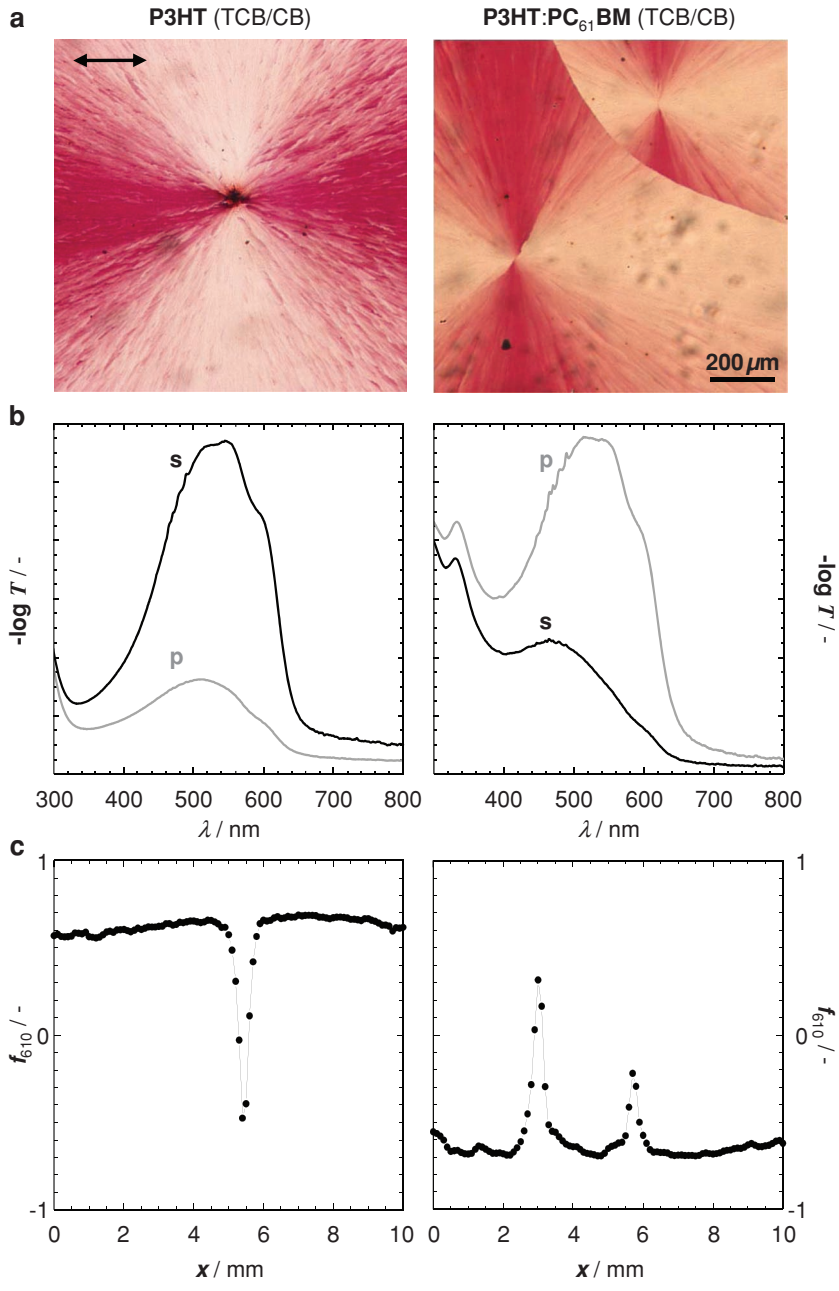

Figure 2. Absorbance of P3HT (left column) and 1:1 P3HT:$PC_{61}BM$ (right column) spin-coated from 7.5 and 10 vol% TCB, respectively. a) Polarized optical micrographs. Orientation of the single polarizer indicated by a black arrow. b) Polarized photometry measurements recorded at a horizontal distance of ≈1 mm from the center of a spherulite-like structure. Polarization direction as indicated (s-polarization horizontal; p-polarization vertical). c) Orientation factor f_{610} at 610 nm as a function of position *x*. The sample was translated horizontally and a polarized photometry measurement was performed every 100 µm; the spot size was approximately 200 µm. Note that the P3HT scan crossed the center of one spherulite-like structure, whereas the 1:1 P3HT:$PC_{61}BM$ scan passed through two centers.

The P3HT and P3HT:$PC_{61}BM$ thin films that were prepared in this study revealed a root-mean-square surface roughness of 32 and 25 nm, respectively (Supporting Information Figure S4). Although these values are relatively large for thin polymer films and might be detrimental for some applications or geometries, we would like to point out that as discussed above Vohra et al. and Zhu et al. were able to prepare solar cells with a bilayer architecture, which comprised a $PC_{61}BM$ layer on top of a rough P3HT film that had been aligned through rubbing.[22,24]

We employed polarized microscopy, photometry, and photoluminescence (PL) spectroscopy to characterize the in-plane molecular orientation of P3HT in the observed spherulite-like structures. When examined in transmission with polarized light the conjugated polymer preferentially absorbs if the backbone lies parallel to the polarizing direction.[32] Accordingly, sections that are red indicate parallel alignment, whereas a colorless appearance implies orthogonal orientation. As can be discerned from the polarized micrographs displayed in **Figure 2**a, P3HT samples feature radial alignment of the polymer backbone. This observation is consistent with previous reports, which have established that the macromolecule crystallizes with the backbone parallel to the fast growth axis c_{TCB} of TCB crystals, i.e., $c_{P3HT} \parallel c_{TCB}$ (**Figure 3**).[8,9,12] Epitaxy occurs due to the close match between the repeat distance of thiophene units $c_{P3HT}/2 \approx 3.8$ Å and $c_{TCB} \approx 3.9$ Å. In the here discussed samples c_{TCB} points radially outward from the center and gives rise to circular symmetric spherulite-like structures. Unexpectedly, in case of P3HT:$PC_{61}BM$ we observe a preferred tangential orientation with the backbone perpendicular to the crystal growth direction, i.e., $c_{P3HT} \perp c_{TCB}$ (cf. below for further discussion of the crystal orientation).

Polarized photometry permitted us to characterize the in-plane optical anisotropy as a function of position with respect to the center of spherulite-like structures. We recorded the transmittance *T* of polarized light during two horizontal scans through the center of a spherulite-like structure and calculated the optical densities according to $A = -\log T$ (Figure 2b). We define the dichroic ratio as $DR = A_s/A_p$ and an orientation factor $f = (DR-1)/(DR+1)$, where A_s and A_p are the recorded optical density for a horizontal (s) and a vertical (p) polarizer setting, respectively. For P3HT, we obtain the highest value $DR_{610} \approx 5$ at a wavelength of 610 nm, which coincides with the absorbance that indicates π-stacking of the polymer, i.e., ordering along the *b*-axis (Supporting Information Figure S5).[30] P3HT:$PC_{61}BM$ samples reveal corresponding behavior. In order to quantify the degree of radial and tangential alignment, we calculated the orientation factor f_{610} at 610 nm and find a similar absolute value of $f_{610} \approx 0.6$ and $f_{610} \approx -0.7$ in case of P3HT and P3HT:$PC_{61}BM$,

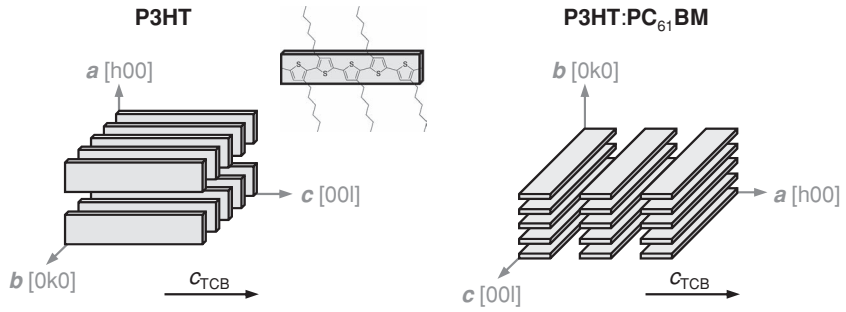

Figure 3. Schematic of the polymer crystal orientation with respect to the fast growth axis c_{TCB} of TCB crystals in P3HT (left) and P3HT:$PC_{61}BM$ thin films (right).

respectively (Figure 2c). Moreover, f_{610} varies little for distances more than 0.5 mm away from the center of spherulite-like structures, which confirms that a high anisotropy is maintained over at least several millimeters. Mapping of the polarized PL confirmed the high optical anisotropy and homogeneity of the prepared spherulite-like structures (**Figure 4**). Using DR = PL_s/PL_p for P3HT and P3HT:$PC_{61}BM$ we obtain at the peak emission wavelength of 720 nm orientation factors with a value of $f_{720} \approx 0.7$ and $f_{720} \approx -0.6$, respectively. In addition, PL spectroscopy permitted us to probe the degree of phase-separation of donor and acceptor molecules in P3HT:$PC_{61}BM$ spherulite-like structures. Comparison of the absolute PL intensity of reference P3HT and blend films indicates a 15-fold quenching of the polymer emission that was recorded with the polarizer parallel to the polymer backbone. This value is comparable to measurements of optimally annealed blends reported in the literature.[33] Therefore, we conclude that processing with TCB does not adversely affect the bulk–heterojunction nanostructure of this blend.

In order to explore the orientation of P3HT crystallites as well as the relative degree of crystallinity (DOC) of the polymer, we recorded a series of grazing-incidence wide-angle X-ray scattering (GIWAXS) patterns (**Figure 5** and **Table 1**). Reference samples that were spin-coated from CB feature a strong diffraction at $q_{020} \approx 1.64$ Å^{-1} as well as a pronounced signal at $q_{100} \approx 0.38$ Å^{-1}. According to the orthorhombic unit cell first proposed by Prosa et al. these two signals correspond to side-chain and π-stacking of P3HT along the *a*- and *b*-axis, respectively.[34] Both, P3HT as well as P3HT:$PC_{61}BM$ films processed from TCB/CB feature additional diffractions that we labeled 220 and 320. Those were first reported by Brinkmann and Rannou for low molecular-weight P3HT crystallized with TCB, who proposed a monoclinic unit cell.[9,11]

We calculated the orientation of crystallites based on the angular distribution of the 100 signal and defined edge-on as a_{P3HT} being within 45° of the substrate normal, whereas face-on is the opposite case with a_{P3HT} lying within 45° of the plane of the substrate.[35,36] Reference P3HT contains 87% of crystallites with edge-on orientation, whereas blend films reveal little preferential texture (**Table 2**). This is in contrast to samples processed from TCB/CB. Whereas for P3HT edge-on and face-on orientation is comparable, blend films are composed of 64% face-on oriented polymer crystallites. Here, we would like to recall that a high degree of out-of-plane π-stacking is desired for P3HT:$PC_{61}BM$ solar cells.[23] Based on the preferential face-on orientation of polymer crystallites in blend films processed from TCB/CB, we conclude that the side-chain stacking distance $a_{P3HT} \parallel c_{TCB}$ (cf. Figure 3) and propose that epitaxy in the P3HT:$PC_{61}BM$ blend is promoted by lattice matching of $a_{P3HT} \approx 15.7$–16.0 Å and $4 \cdot c_{TCB} \approx 15.6$ Å.[9–11,37,38]

We constructed a set of pole figures based on the 100 signal to extract the relative degree of crystallinity (DOC) of the polymer, which is summarized in Table 2 (see Supporting Information Figure S6 for pole figures).[35,36] Reference P3HT features the highest crystallinity of all investigated samples, which we set equal to 1. In contrast, P3HT films spin-coated from 7.5 vol% TCB are less ordered as evidenced by the much lower DOC ≈ 0.32. This can be explained by a reduction in the period of time available for solidification due to rapid solvent removal during growth of TCB crystals. P3HT:$PC_{61}BM$ blends display the opposite behavior. Reference blend films are largely disordered, which is consistent with the strong tendency of this system to form glassy solids.[39] Thus, processing from TCB/CB doubles the relative degree of crystallinity of P3HT in blend films to DOC ≈ 0.30 despite rapid solidification. The comparable DOC as well as the presence of a monoclinic P3HT unit cell in both neat and blend films processed from TCB/CB suggests similar solidification behavior.

Moreover, the shape of the recorded GIWAXS pole figures provides information about the nucleation of P3HT crystallites (Supporting Information Figure S6). Generally, a sharp central peak indicates the presence of highly oriented crystallites on the substrate. We observe this feature in reference P3HT and P3HT:$PC_{61}BM$ films, which previously has been associated with substrate nucleation of this polymer.[40] In contrast, this signal is not present in samples processed from TCB/CB, which indicates that growth of P3HT crystals instead commences throughout the bulk of thin films. We explain the absence of substrate nucleation by exclusive epitaxial solidification of P3HT on TCB crystals.

In some cases uniaxial orientation might be preferred rather than the circular symmetry of spherulite-like structures. Thus we explored, whether uniaxial orientation can be introduced by other solution deposition methods. We selected dip-coating as a proof-of-principle method. A substrate was submerged in a TCB/CB solution of P3HT (8 vol% TCB) and then slowly removed at a rate of about 50 cm min^{-1}, which approximately coincides with the rate of drying of the carrier solvent CB. This resulted in a directed drying gradient that led to directional solidification of the semiconductor during film formation from solution. We obtained films that displayed a high degree of optical anisotropy, as evidenced by the polarized optical micrographs shown in **Figure 6**a. Gratifyingly, visual inspection confirmed that the orientation is maintained over an area of several square centimeters. We argue that the use of a crystallizable solvent mixture with other large-area deposition methods is likely to provide a similar result. For instance, graded solvent removal is a common feature of zone-casting,[41] blade-coating[42,43] and inkjet-printing.[44]

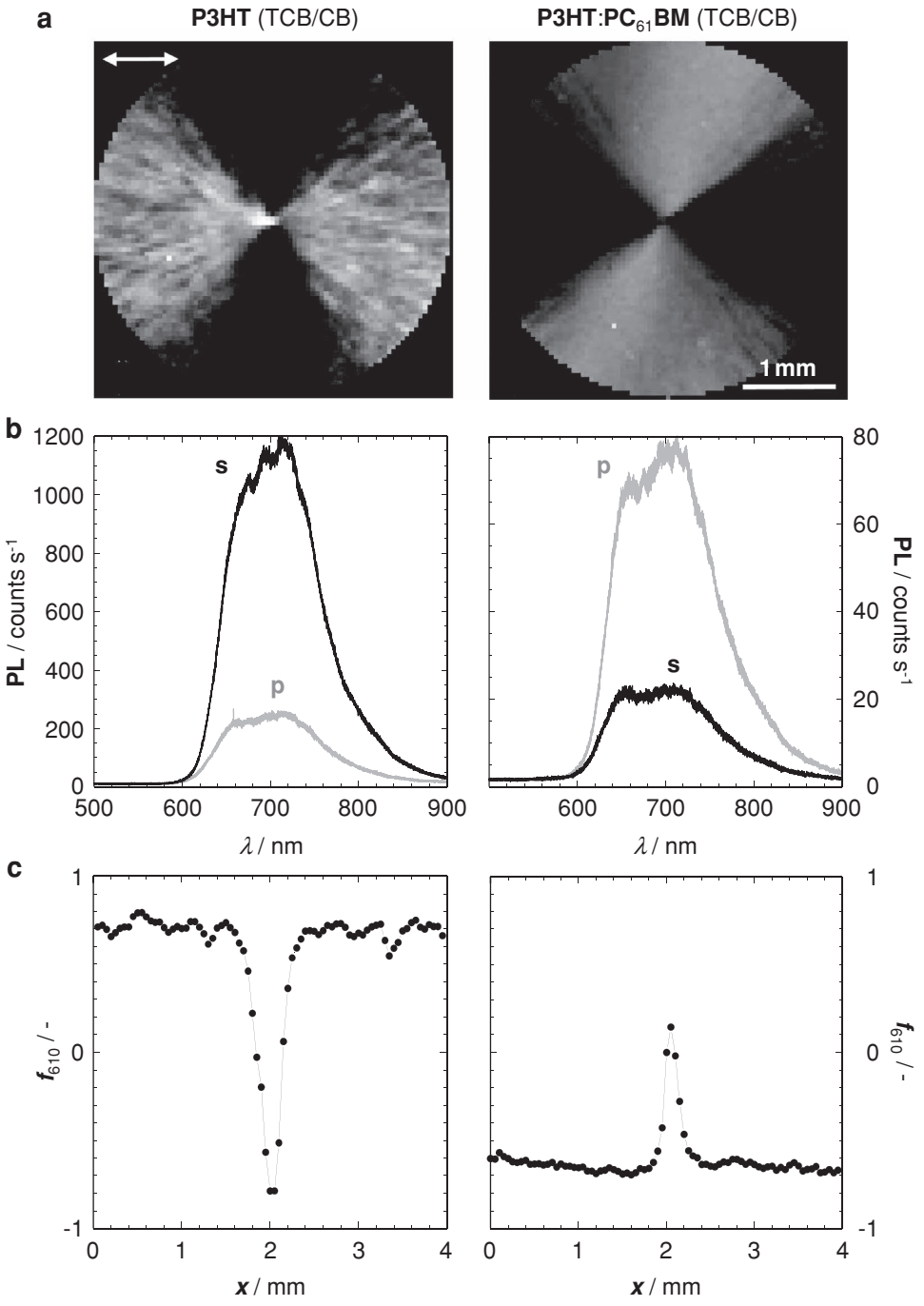

Figure 4. Photoluminescence of P3HT (left column) and 1:1 P3HT:$PC_{61}BM$ (right column) spin-coated from 7.5 and 10 vol% TCB, respectively. a) Maps of polarized PL at 720 nm that were recorded with the center of a spherulite-like structure at the origin. Orientation of the single polarizer indicated by a white arrow. b) PL spectra recorded at a horizontal (s, black) and vertical (p, gray) distance of ≈1 mm from the center of spherulite-like structures. The absolute PL intensity is shown. c) Orientation factor f_{720} at 720 nm as a function of position *x*. The sample was translated horizontally and a polarized PL measurement was performed every 50 µm; the spot size was approximately 50–100 µm.

For some applications, the growth of macroscopic single-crystal-like entities may be of interest. Here, crystallization from solutions that contain an excess of the crystallizable solvent can be used. We observe that P3HT solidified from a solution, which contained about 50 vol% TCB, forms millimeter long needles that feature uniaxial orientation of the macromolecule, as judged by the optical micrographs displayed in Figure 6b.

Finally, we explored the applicability of the here proposed method to other semiconductor systems, the results of which are summarized in **Table 3**. Amorphous, regio-random P3HT

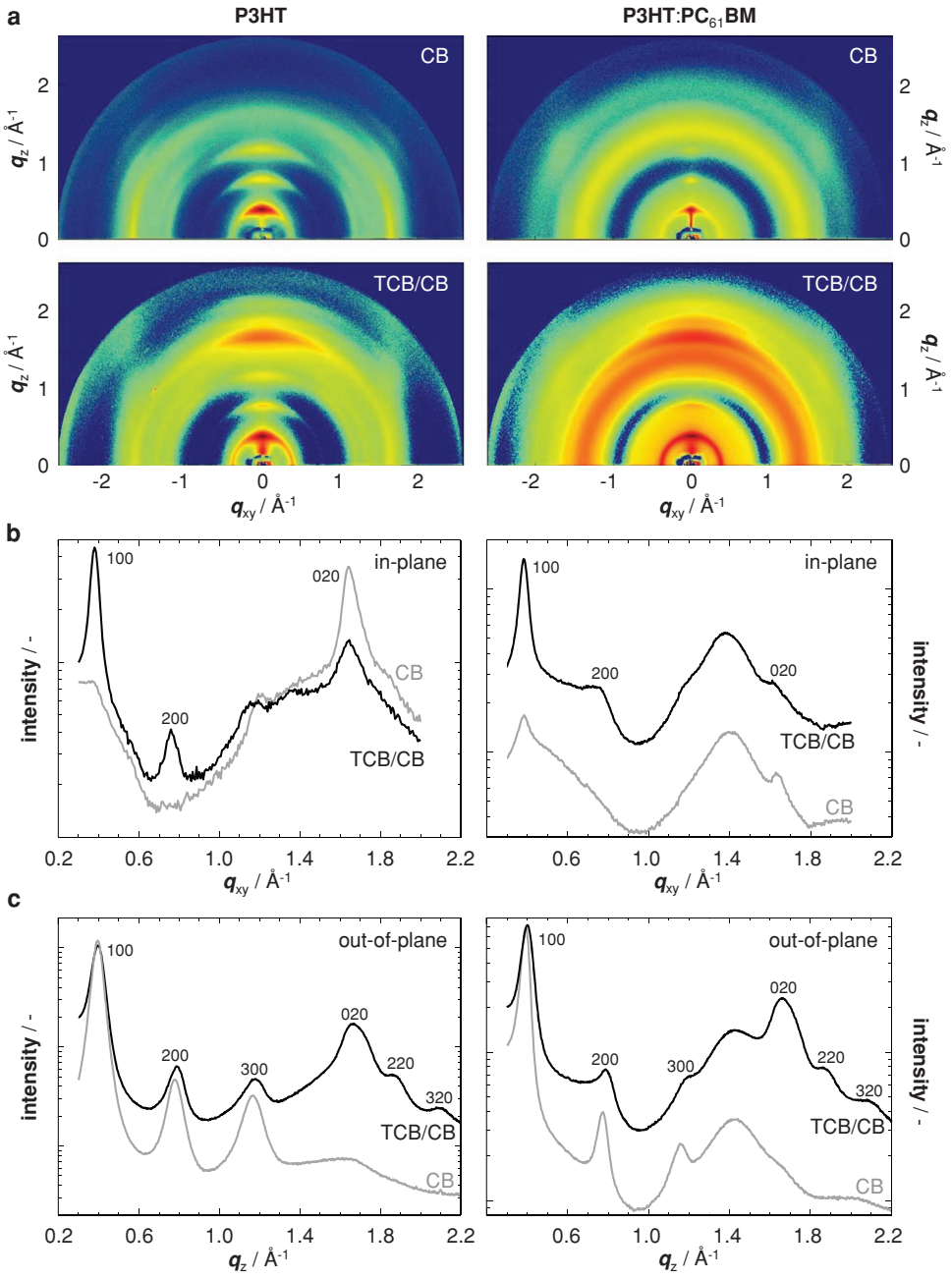

Figure 5. Grazing-incidence wide-angle X-ray scattering (GIWAXS) of P3HT (left column) and 1:1 P3HT:$PC_{61}BM$ (right column) spin-coated from CB as well as TCB/CB (7.5 and 10 vol% TCB, respectively). a) GIWAXS patterns of reference samples spin-coated from CB (top) and TCB/CB thin films (bottom). Diffractograms with the scattering vector q_{xy} in-plane (b) and q_z out-of-plane (c) with respect to the substrate: spin-coated from CB (gray) and TCB/CB (black). The diffractions are labeled according to the orthorhombic (CB) or monoclinic (TCB/CB) unit cell of P3HT, respectively.

(ra-P3HT) that was spin-coated from a 7.5 vol% TCB solution continued to display a featureless appearance in cross-polarized optical microscopy (not shown). In contrast, we were able to produce thin-film spherulite-like structures with a variety of materials that show a tendency to π-stack. Those include a number of conjugated polymers, *i.e.,* P3BT, P3DDT, PCPDTBT, PFO and F8BT, the small molecule EH-DPP-TFPV as well as selected polymer:fullerene and polymer:polymer blends (*cf.* Supporting Information Figure S7 and Experimental section for detailed chemical structures). These materials systems exhibit different phase behavior ranging from liquid-crystalline to semi-crystalline, and are used for a wide range of applications including organic LEDs, transistors, photodetectors and polymer solar cells. We would like to highlight in particular the small band-gap polymer PCPDTBT, which has been extensively investigated for polymer solar cells. PCPDTBT:$PC_{71}BM$

Table 1. Peak GIWAXS signals obtained from diffractograms displayed in Figure 5. Signals for P3HT (and in brackets for P3HT:$PC_{61}BM$) are shown.

	CB		TCB/CB	
	in-plane, q_{xy} [Å^{-1}]	out-of-plane, q_z [Å^{-1}]	in-plane, q_{xy} [Å^{-1}]	out-of-plane, q_z [Å^{-1}]
100	0.37 (0.38)	0.39 (0.39)	0.38 (0.38)	0.40 (0.40)
200	–	0.78 (0.77)	0.76 (0.72)	0.79 (0.79)
300	–	1.17 (1.16)	–	1.18 (1.20)
020	1.64 (1.63)	–	1.65 (1.61)	1.67 (1.66)
220	–	–	–	1.86 (1.86)
320	–	–	–	2.09 (2.08)

bulk–heterojunction blends offer a promising photovoltaic performance provided that the nanostructure is carefully controlled. Previously, this has been achieved by using processing additives such as 1,8-octanedithiol,[29,45] which assists ordering of the polymer during film formation.[46] Processing with TCB results in well-defined spherulite-like structures in PCPDTBT as well as PCPDTBT:$PC_{71}BM$ thin films (*cf.* Table 3). Similar to the P3HT system discussed above, we observe radial alignment of the polymer in PCPDTBT samples, whereas blend films feature tangential orientation (not shown). We employed GIWAXS to further examine this system and found that the crystallizable solvent increases the face-on orientation of the polymer backbone in PCPDTBT thin films, as evidenced by the strong out-of-plane π-stacking signal at $q_{010} \approx 1.65$ Å^{-1} that is almost completely absent in the in-plane scan (Supporting Information Figure S8). Unfortunately, we were unable to distinguish polymer diffractions in corresponding blend samples.

3. Conclusions

We have demonstrated that the crystallizable solvent technique can be employed to align conjugated polymer systems. In addition, we were able to modify this method to achieve the one-step preparation of thin films that feature pronounced in-plane alignment. The material is dissolved together with the crystallizable solvent TCB in a second carrier solvent, e.g., CB. This solution can be deposited by spin- or dip-coating, which results in highly ordered and continuous thin films. Depending on the processing method, we observe macroscopic domains, which are composed of one spherulite-like structure each, or uniaxial alignment of the macromolecule. Besides a variety of semi-crystalline conjugated polymers and small molecules, this approach is applicable to a number of polymer:fullerene and polymer:polymer bulk–heterojunction blends. Thus, the

Table 2. Relative degree of crystallinity (DOC) of the bulk, substrate interface and total thin film; degree of edge-on and face-on orientation of P3HT crystallites.

	P3HT		P3HT:$PC_{61}BM$	
	CB	TCB/CB	CB	TCB/CB
bulk DOC [a.u.]	0.98	0.32	0.15	0.30
interface DOC [a.u.]	0.17	0.00	0.09	0.00
total DOC [a.u.]	1.00	0.32	0.15	0.30
% edge-on	87	56	54	36
% face-on	13	44	46	64

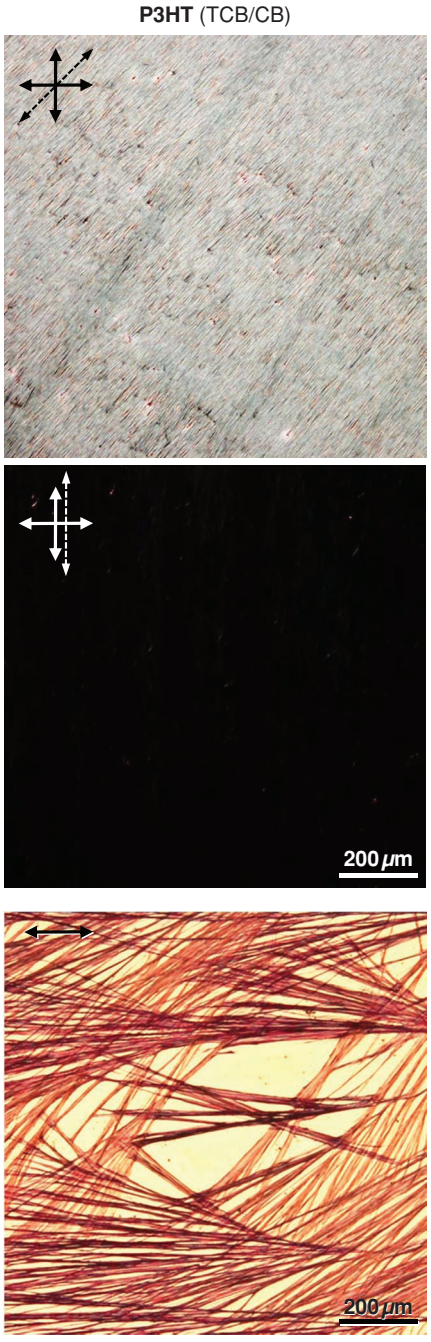

Figure 6. Dip-coating and single-crystal like entities. (a) Cross-polarized optical micrographs of P3HT dip-coated from 8 vol% TCB with the dip-coating direction at 45° (top) and 0° (bottom) with respect to the analyzer. Orientation of the polarizer pair indicated by solid arrows; dip-coating direction indicated with dashed arrows. (b) Polarized optical micrograph of P3HT spin-coated from ≈50 vol% TCB. Orientation of the single polarizer indicated by a black arrow.

Table 3. Cross-polarized micrographs (1.2 cm^2) of various organic semiconductor and blend thin films spin-coated from CB and TCB/CB (7.5 vol% TCB for single semiconductor films; 10 vol% for blend films).

material	cross-polarized micrographs	
	CB	TCB/CB
P3BT		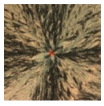
1:1 P3BT:PC_{61}BM		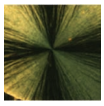
P3DDT		
1:1 P3DDT:PC_{61}BM		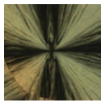
PCPDTBT	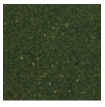	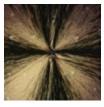
1:2 PCPDTBT:PC_{71}BM		
PFO		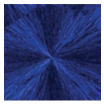
F8BT		
17:2:1 PFO:F8BT:MEH-PPV[a)]		
EH-DPP-TFPV[a)]		

[a)]The PFO:F8BT:MEH-PPV and EH-DPP-TFPV samples were spin-coated from chloroform and TCB/chloroform (7.5 vol% TCB).

here developed technique could be of benefit for a wide range of opto-electronic applications and may offer a straightforward processing routine for the realization of concepts such as polarizing organic photovoltaics. In addition, we found that the use of a crystallizable solvent promotes polymer crystallization in a similar way as thermal annealing or the use of processing additives such as alkanedithiols, which are frequently employed for the optimization of polymer solar cells.

4. Experimental Section

Materials: All materials were used as received by the following suppliers. Sigma-Aldrich: regio-regular poly(3-butylthiophene-2,5-diyl) (P3BT; $M_n \approx 23$ kg mol^{-1}, $M_w \approx 54$ kg mol^{-1}, regio-regularity ≈ 90%), regio-regular poly(3-hexylthiophene-2,5-diyl) (P3HT; $M_n \approx 21$ kg mol^{-1}, $M_w \approx 48$ kg mol^{-1}, region-regularity ≈ 90%), regio-regular poly(3-dodecylthiophene-2,5-diyl) (P3DDT; $M_n \approx 35$ kg mol^{-1}, $M_w \approx 49$ kg mol^{-1}, region-regularity ≈ 90%), regio-random P3HT (ra-P3HT, molecular weight not provided by supplier), poly(9,9-di-n-octylfluorenyl-2,7-diyl) (PFO; $M_n \approx 23$ kg mol^{-1}, $M_w \approx 83$ kg mol^{-1}), poly[(9,9-di-*n*-octylfluorenyl-2,7-diyl)-*alt*-(benzo[2,1,3]thiadiazol-4,8-diyl)] (F8BT; $M_n \approx 6$ kg mol^{-1}, $M_w \approx 14$ kg mol^{-1}), chlorobenzene (CB; purity ≈ 99%) and 1,3,5-trichlorobenzene (TCB; purity ≈ 99%). 1-Material: poly[2,6-(4,4-bis-(2-ethylhexyl)-4*H*-cyclopenta[2,1-b;3,4-b′]dithiophene)-alt-4,7(2,1,3-benzothiadiazole)] (PCPDTBT; $M_n \approx 11$ kg mol^{-1}, $M_w \approx 25$ kg mol^{-1}) and poly[2-methoxy-5-(2-ethylhexyloxy)-1,4-phenylenevinylene] (MEH-PPV; $M_n \approx 23$ kg mol^{-1}, $M_w \approx 80$ kg mol^{-1}). Solenne BV: [6,6]-phenyl-C_{61}-butyric acid methyl ester (PC_{61}BM) and [6,6]-phenyl-C_{71}-butyric acid methyl ester (PC_{71}BM). Compound 2,5-bis(2-ethylhexyl)-1,4-bis[5-[(E)-2-[4-(trifluoromethyl) phenyl]vinyl]-2-thienyl]pyrrolo[3,4-c]pyrrole-3,6-dione (EH-DPP-TFPV) was synthesized according to Ref [47].

Sample Preparation: Organic semiconductor thin films were spin-coated from chlorobenzene (CB) solution that contained a varying amount of 1,3,5-trichlorobenzene (TCB; spin-coating speed 1000 rpm). Polymer solutions contained 20 g L^{-1} of polymer (10 g L^{-1} for dip-coating); polymer:fullerene solutions contained 40 g L^{-1} of blend material. Samples were prepared on microscopy glass slides (cleaned with water, acetone and isopropyl alcohol) for optical microscopy, AFM as well as photometry and silicon wafers with a native silicon oxide layer for PL spectroscopy and GIWAXS. Subsequently, samples were stored in a desiccator to remove residual solvent. The film thickness was measured with a P16+ surface profilometer from KLA Telcor.

Optical Microscopy: Optical microscopy was carried out with an Olympus BX51 polarizing microscope using a 5× objective.

Atomic Force Microscopy (AFM): AFM measurements were performed with an Agilent 5500 SPM (Molecular Imaging) instrument. Topographical images were recorded in tapping mode using a silicon cantilever (FM-50) with a resonance frequency of 75 kHz.

UV-vis absorbance spectroscopy: UV-vis spectra were recorded with a Perkin Elmer Lambda 900 UV-vis spectrophotometer.

Attenuated Total Reflectance Infrared (ATR-IR) Spectroscopy: ATR-IR spectra were recorded with a Spectrum One FTIR Spectrometer equipped with a Universal Attenuated Total Reflectance Sampling Accessory.

Photoluminescence (PL) Spectroscopy: PL spectra were collected with a Lab Ram HR800 system coupled to a nitrogen-cooled UV-enhanced CCD detector in backscattering geometry using the 405 nm line from a solid state laser. Mapping of PL emission was performed at ambient temperature with a motorized XY translation stage (step size 50 µm; spot size 50–100 µm). A nitrogen-flushed sample stage was used.

Polarized Photometry: Polarized photometry was performed using a SOPRALAB rotating polarizer ellipsometer (GES-5E) coupled to a CCD detector.

Grazing-Incidence Wide-Angle X-ray Scattering (GIWAXS): GIWAXS was performed at the Stanford Synchrotron Radiation Lightsource (SSRL) on beam line 7-2 (high resolution grazing incidence), 2-1 (high resolution specular data), and 11-3 (2D scattering with an area detector, MAR345 image plate, at grazing incidence). The incident energy was 8 keV for beam lines 7-2 and 2-1, and 12.7 keV for beam line 11-3. The diffracted beam was collimated with 1 milliradian Söller slits for high resolution in-plane scattering and with two 1 mm slits for specular diffraction. For both grazing-incidence experiments, the incidence angle was slightly larger than the critical angle in order to ensure that the full film depth was sampled. Scattering data are expressed as a function of the scattering vector $q = 4\pi \cdot \sin(\theta)/\lambda$, where θ is half the scattering angle and λ is the wavelength of the incident radiation. Here, q_{xy} and q_z are the components of the scattering vector that are parallel and perpendicular to the substrate, respectively. For details of the pole figure construction and

calculation of the crystal orientation and relative degree of crystallinity DOC, see Refs. [35,36].

Supporting Information

Supporting Information is available from the Wiley Online Library or from the author.

Acknowledgements

The authors thank the Ministerio de Economía y Competitividad for generous funding through projects MAT2009-10642, PLE2009-0086 and RYC-2009-05392. C.M. gratefully acknowledges financial support from the CSIC through the JAE-Doc program (European Social Fund). We are indebted to Mr. B. Dorling (ICMAB) for assistance with dip-coating. P.S. acknowledges the Visiting Investigatorship Programme (VIP) of the Agency for Science, Technology and Research (A*STAR), Republic of Singapore for financial support. Supporting Information is available online from Wiley InterScience or from the author.

Received: October 13, 2012
Published online: January 3, 2013

[1] *Organic Photovoltaics: Materials, Device Physics, and Manufacturing Technologies* (Eds: C. Brabec, U. Scherf, V. Dyakonov), Wiley-VCH, Weinheim **2008**.
[2] *Flexible Electronics: Materials and Applications* (Eds: W. S. Wong, A. Salleo), Springer, New York **2009**.
[3] *Organic Electronics II: More Materials and Applications* (Ed: H. Klauk), Wiley-VCH, Weinheim **2012**.
[4] M. Grell, D. D. C. Bradley, M. Inbasekaran, E. P. Woo, *Adv. Mater.* **1999**, *9*, 798–802.
[5] H. Sirringhaus, R. J. Wilson, R. H. Friend, M. Inbasekaran, W. Wu, E. P. Woo, M. Grell, D. D. C. Bradley, *Appl. Phys. Lett.* **2000**, *77*, 406–408.
[6] J. C. Wittmann, P. Smith, *Nature* **1991**, *352*, 414–417.
[7] X. L. Chen, Z. Bao, B. J. Sapjeta, A. J. Lovinger, B. Crone, *Adv. Mater.* **2000**, *12*, 344–347.
[8] M. Brinkmann, J. C. Wittmann, *Adv. Mater.* **2006**, *18*, 860–863.
[9] M. Brinkmann, P. Rannou, *Adv. Funct. Mater.* **2007**, *17*, 101–108.
[10] M. Brinkmann, *Macromolecules* **2007**, *40*, 7532–7541.
[11] N. Kayunkid, S. Uttiya, M. Brinkmann, *Macromolecules* **2010**, *43*, 4961–4967.
[12] L. H. Jimison, M. F. Toney, I. McCulloch, M. Heeney, A. Salleo, *Adv. Mater.* **2009**, *21*, 1568–1572.
[13] M. Hamaguchi, K. Yoshino, *Appl. Phys. Lett.* **1995**, *67*, 3381–3383.
[14] P. Dyreklev, G. Gustafsson, O. Inganäs, H. Stubb, *Solid State Commun.* **1992**, *82*, 317–320.
[15] P. Dyreklev, M. Berggren, O. Inganäs, M. R. Andersson, O. Wennerström, T. Hjertberg, *Adv. Mater.* **1995**, *7*, 43–45.
[16] B. O'Connor, R. J. Kline, B. R. Conrad, L. J. Richter, D. Gundlach, M. F. Toney, D. M. DeLongchamp, *Adv. Funct. Mater.* **2011**, *21*, 3697–3705.
[17] Z. Zheng, K.-H. Yim, M. S. M. Saifullah, M. E. Welland, R. H. Friend, J.-S. Kim, W. T. S. Huck, *Nano Lett.* **2007**, *7*, 987–992.
[18] Z. Hu, B. Muls, L. Gence, D. A. Serban, J. Hofkens, S. Melinte, B. Nysten, S. Demoustier-Champagne, A. M. Jonas, *Nano Lett.* **2007**, *7*, 3639–3644.
[19] V. Cimrová, M. Remmers, D. Neher, G. Wegner, *Adv. Mater.* **1996**, *8*, 146–149.
[20] E. J. W. Crossland, K. Rahimi, G. Reiter, U. Steiner, S. Ludwigs, *Adv. Funct. Mater.* **2011**, *21*, 518–524.
[21] E. J. W. Crossland, K. Tremel, F. Fischer, K. Rahimi, G. Reiter, U. Steiner, S. Ludwigs, *Adv. Mater.* **2012**, *24*, 839–844.
[22] V. Vohra, G. Arrighetti, L. Barba, K. Higashimine, W. Porzio, H. Murata, *J. Phys. Chem. Lett.* **2012**, *3*, 1820–1823.
[23] E. D. Gomez, K. P. Barteau, H. Wang, M. F. Toney, Y.-L. Loo, *Chem. Commun.* **2011**, *47*, 436–438.
[24] R. Zhu, A. Kumar, Y. Yang, *Adv. Mater.* **2011**, *23*, 4193–4198.
[25] K. Vandewal, K. Tvingstedt, O. Inganäs, *Phys. Rev. B* **2012**, *86*, 035212.
[26] J. C. Wittmann, B. Lotz, *Prog. Polym. Sci.* **1990**, *15*, 909–948.
[27] Initially, we measured the TCB content by weight and then used the density of 1,2,4-trichlorobenzene $\rho_{1,2,4\text{-TCB}}$=1.45 g mL^{-1}, which is a liquid at ambient, to calculate the volume fraction.
[28] A. J. Moulé, K. Meerholz, *Adv. Mater.* **2008**, *20*, 240–245.
[29] Y. Yao, J. Hou, Z. Xu, G. Li, Y. Yang, *Adv. Funct. Mater.* **2008**, *18*, 1783–1789.
[30] J. Clark, C. Silva, R. H. Friend, F. C. Spano, *Phys. Rev. Lett.* **2007**, *98*, 206406.
[31] A. Keawprajak, P. Piyakulawat, A. Klamchuen, P. Iamraksa, U. Asawapirom, *Sol. Energy Mater. Sol. Cells* **2010**, *94*, 531–536.
[32] M. C. Gurau, D. M. DeLongchamp, B. M. Vogel, E. K. Lin, D. A. Fischer, S. Sambasivan, L. J. Richter, *Langmuir* **2007**, *23*, 834–842.
[33] Y. Kim, S. Cook, S. M. Tuladhar, S. A. Choulis, J. Nelson, J. R. Durrant, D. D. C. Bradley, M. Giles, I. McCulloch, C.-S. Ha, M. Ree, *Nat. Mater.* **2006**, *5*, 197–203.
[34] T. J. Prosa, M. J. Winokur, J. Moulton, P. Smith, A. J. Heeger, *Macromolecules* **1992**, *25*, 4364–4372.
[35] J. L. Baker, L. H. Jimison, S. Mannsfeld, S. Volkman, S. Yin, V. Subramanian, A. Salleo, A. P. Alivisatos, M. F. Toney, *Langmuir* **2010**, *26*, 9146–9151
[36] L. H. Jimison, *Understanding Microstructure and Charge Transport in Semicrystalline Polythiophenes*, PhD Thesis, Stanford University **2011**.
[37] Z. Wu, A. Petzold, T. Henze, T. Thurn-Albrecht, R. H. Lohwasser, M. Sommer, M. Thelakkat, *Macromolecules* **2010**, *43*, 4646–4653.
[38] Note that compared to the orthorhombic P3HT unit cell (cf. Ref. [34]) the monoclinic unit cell features a shortened side-chain *a*-spacing (cf. Refs. [9–11,37]).
[39] C. Müller, T. A. M. Ferenczi, M. Campoy-Quiles, J. M. Frost, D. D. C. Bradley, P. Smith, N. Stingelin-Stutzmann, J. Nelson, *Adv. Mater.* **2008**, *20*, 3510–3515.
[40] R. J. Kline, M. D. McGehee, M. F. Toney, *Nat. Mater.* **2006**, *5*, 222–228.
[41] W. Pisula, A. Menon, M. Stepputat, I. Lieberwirth, U. Kolb, A. Tracz, H. Sirringhaus, T. Pakula, K. Müllen, *Adv. Mater.* **2005**, *17*, 684–689.
[42] T. Wang, A. D. F. Dunbar, P. A. Staniec, A. J. Pearson, P. E. Hopkinson, J. E. MacDonald, S. Lilliu, C. Pizzey, N. J. Terrill, A. M. Donald, A. J. Ryan, R. A. L. Jones, D. G. Lidzey, *Soft Matter* **2010**, *6*, 4128–4134.
[43] M. Sanyal, B. Schmidt-Hansberg, M. F. G. Klein, A. Colsmann, C. Munuera, A. Vorobiev, U. Lemmer, W. Schabel, H. Dosch, E. Barrena, *Adv. Energy Mater.* **2011**, *1*, 363–367.
[44] S. T. Beyer, K. Walus, *Langmuir* **2012**, *28*, 8753–8759.
[45] J. Peet, J. Y. Kim, N. E. Coates, W. L. Ma, D. Moses, A. J. Heeger, G. C. Bazan, *Nat. Mater.* **2007**, *6*, 497–500.
[46] T. Agostinelli, T. A. M. Ferenczi, E. Pires, S. Foster, A. Maurano, C. Müller, A. Ballantyne, M. Hampton, S. Lilliu, M. Campoy-Quiles, H. Azimi, M. Morana, D. D. C. Bradley, J. Durrant, J. E. Macdonald, N. Stingelin, J. Nelson, *J. Polym. Sci., Part B: Polym. Phys.* **2011**, *49*, 717–724.
[47] W. Kylberg, P. Sonar, J. Heier, J.-N. Tisserant, C. Müller, F. Nüesch, Z.-K. Chen, A. Dodabalapur, S. Yoon, R. Hany, *Energy Environ. Sci.* **2011**, *4*, 3617–3624.